

Tuning of coupling modes in laterally parallel double open quantum dots

Chi-Shung Tang,¹ Wing Wa Yu,² and Vidar Gudmundsson²

¹*Physics Division, National Center for Theoretical Sciences, P.O. Box 2-131, Hsinchu 30013, Taiwan*

²*Science Institute, University of Iceland, Dunhaga 3, IS-107 Reykjavik, Iceland*

We consider electronic transport through laterally parallel double open quantum dots embedded in a quantum wire in a perpendicular magnetic field. The coupling modes of the dots are tunable by adjusting the strength of a central barrier and the applied magnetic field. Probability density and electron current density are calculated to demonstrate transport effects including magnetic blocking, magnetic turbulence, and a hole-like quasibound state feature. Fano to dip line-shape crossover in the conductance is found by varying the magnetic field.

PACS numbers: 73.23.-b, 73.21.La, 73.21.Hb, 85.35.Ds

I. INTRODUCTION

Electronic transport through an open quantum dot has attracted broad attention^{1,2,3,4,5,6,7,8,9,10,11,12} due to its potential in the investigation of various bound-state features,⁸ phase coherence,^{9,10} and wave function imaging.^{11,12} In high electron mobility samples at low temperatures, the electron phase coherent length may be longer than the dimension of the open dot system, allowing electrons to remain coherent while traversing the system with negligible impurity effects. Moreover, since the outgoing electrons from the open dot are strongly coupled to reservoirs without tunneling, the Coulomb effects are negligible.

By coupling two quantum dots in series or in parallel, a double quantum dot is formed.^{13,14,15,16} Quantum transport through such a double dot system has attracted considerable attention due to its versatility for various applications.^{17,18,19,20,21,22,23,24,25,26} The double dot system provides possible new mechanism compared to a single quantum dot as electrons could be coupled between the two dots, thus forming an artificial quantum dot molecular junction.^{17,18,19} In addition, the coupled dot system is likely to be important in quantum information processing,^{20,21,22,23} where external field manipulation and quantum coherence are both required. Thus far these coupled dot systems are, however, assumed to be isolated and can be described by an Anderson-type model.^{24,25,26}

We would like to emphasize that the adiabaticity of the dot-lead connection holds only for large quantum dots. As the dot size shrinks and approaches the realm of the Fermi wave length, the dot-lead connection no longer remains adiabatic. Experimental findings in electronic transport through quantum dots, such as the individual eigenstates of isolated dot²⁷ and the recurrence of specific groups of wave function scars in the dot,⁶ indicate unequivocally the mode-mixed scattering at the dot-lead connections. It has been shown that the embedded quantum structures can lead to a complicated mode mixing.^{28,29}

In this paper we study the tuning of coupling modes of parallel double open quantum dots (DOQDs) embedded in a quantum wire. The mode-coupling in this system is

coherently adjusted by a central elongated potential barrier separating the system into upper and lower channels, as depicted in Fig. 1. In addition, an external perpendicular magnetic field is applied to manipulate the electronic cyclotron motion and the coupling between the upper dot (UD) and the lower dot (LD). It is important to note that since the DOQD system is strongly coupled to the source and drain reservoirs, the quantum interference effects are strong and cannot be treated like an isolated dot using Anderson-type model or solving the rate equation for the Fock-Darwin spectrum.³⁰ Here we employ Lippmann-Schwinger approach^{28,29} that allows us to handle a wide range of smooth scatterers embedded in a wire and access the electron probability distribution as well as the electron current flow in the system.

One robust transport phenomenon in open quantum structures is the quasibound-state feature with positive^{31,32} or negative^{33,34} binding energy. Indeed, the transport properties of a wire with either static or time-dependent scatterers can exhibit significant quasibound-state features.^{31,32,33,34,35} In a laterally parallel DOQD system, operating the central barrier simultaneously adjusts the dot-dot and dot-lead coupling and tilts the po-

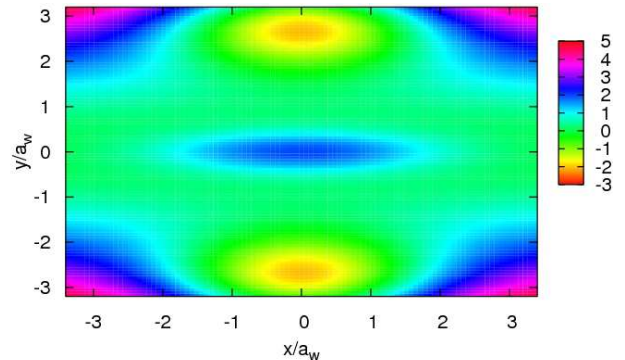


FIG. 1: Schematic illustration of the laterally parallel DOQD system containing two open quantum dots (yellow) to the sides and a central barrier (blue). The color scale on the right shows the potential height in meV. The parameters are $a_w = 33.7$ nm, $\hbar\Omega_0 = 1.0$ meV, $V_1 = V_3 = -6.0$ meV, and $V_2 = 2.0$ meV.

tential of the side dots to affect the alignment of the electron energy with the discrete levels in the dots. The electronic transport thus manifests different types of resonant features.

II. MODEL: A LIPPMANN-SCHWINGER APPROACH

The system under investigation is composed of a laterally parallel DOQD embedded in a quantum wire with confining potential $V_c(y) = \frac{1}{2}m^*\Omega_0^2 y^2$, and hence the electrons are transported through the wire with characteristic energy scale $\hbar\Omega_0$ in the transverse direction. The parallel double open quantum dots are separated by a central barrier that can be used to tune the dot coupling and adjust the mode mixing between the wire subbands and the dot levels. The electrons incident from the left reservoir impinge on the parallel DOQD system modeled by the Gaussian-type scattering potential

$$V_{sc}(x, y) = \sum_{i=1}^3 V_i \exp\left[-\alpha x^2 - \beta_i (y - y_i)^2\right]. \quad (1)$$

Here V_1 and V_3 are negative indicating, respectively, the depth of the UD and the LD, and V_2 is positive describing the height of the central barrier. The three potentials have the same length (same α) while the central barrier is a little narrower than the two dots ($\beta_1 = \beta_3 < \beta_2$) so that the UD is allowed to couple with the LD. In a perpendicular magnetic field $\mathbf{B} = B\hat{z}$, the parabolic confinement defines an effective magnetic length $a_w = (\hbar/m^*\Omega_w)^{1/2}$ in the wire and the subband energy levels

$$E_n = \left(n + \frac{1}{2}\right) \hbar\Omega_w + \frac{(ka_w)^2 (\hbar\Omega_0)^2}{2 \hbar\Omega_w}, \quad (2)$$

where k is the magnitude of the electron wave vector along the wire and $n = 0, 1, \dots$. This defines the effective subband separation $\hbar\Omega_w$, where $\Omega_w^2 = \omega_c^2 + \Omega_0^2$ is related to the cyclotron frequency $\omega_c = eB/(m^*c)$ and the characteristic frequency Ω_0 for the parabolic model. We assume a value of $m^* = 0.067m$ for the effective mass of an electron in GaAs-based material.

In the following we employ a mixed momentum-coordinate presentation³⁶

$$\Psi_E(p, y) \equiv \int dx e^{-ipx} \psi_E(x, y) \quad (3)$$

and utilize a channel-mode expansion $\Psi_E(p, y) = \sum_n \varphi_n(p) \phi_n(p, y)$ to obtain a set of coupled Lippmann-Schwinger integral equations in the momentum space. As such, these equations can then be transformed into integral equations for the T -matrix to facilitate numerical calculation.²⁸ According to the Landauer-Büttiker formalism the energy dependence of the conductance can be calculated²⁸

$$G(E) = G_0 \text{Tr} [\mathbf{t}^\dagger(E) \mathbf{t}(E)] \quad (4)$$

with the conductance quantum $G_0 = 2e^2/h$. Furthermore, with the scattering wave function obtained from the T -matrix we calculate in configuration space the probability density $|\psi_E(x, y)|^2$ and the electron current density

$$\mathbf{J} = \frac{e}{m} \text{Re} \left[\psi_E^* \left(\mathbf{p} + \frac{e}{c} \mathbf{A} \right) \psi_E \right] \quad (5)$$

to clearly demonstrate the transport mechanism and provide detailed insight into the coupling nature of the parallel DOQD system. Here $-e$ is the charge of an electron. For embedded wire systems it is convenient to choose the vector potential $\mathbf{A} = (-By, 0, 0)$ in a Landau gauge.

III. RESULTS AND DISCUSSION

To study the transport behavior in a laterally parallel DOQD system, we consider a broad parabolic wire with confinement energy $\hbar\Omega_0 = 1.0$ meV. This energy corresponds to $a_w = 33.7$ nm in zero magnetic field. In the DOQD system, the central barrier and the side dots have the same effective length $L \simeq 141$ nm ($\alpha = 2 \times 10^{-4}$ nm⁻²), while the width of the central barrier ($\beta_2 = 4 \times 10^{-3}$ nm⁻²) is narrower than the side dots ($\beta_1 = \beta_3 = 0.7 \times 10^{-3}$ nm⁻²) to facilitate the UD-LD coupling. By choosing these parameters, the effective width of the central barrier and the side dots are, respectively, $W_{CB} \simeq 32$ nm and $W_{SD} \simeq 76$ nm. The two open dots have the same potential depth $V_1 = V_3 = -6.0$ meV and are separated by 100 nm from the central barrier ($y_2 = 0$), namely, $y_1 = -y_3 = 100$ nm.

In performing the numerical calculation, a sufficient total number of quantum channels including evanescent modes in momentum space is needed to satisfy the conservation of current condition. Numerical accuracy is assured by comparing the data obtained from a larger basis set. In order to investigate the characteristics of the energy-dependent conductance $G(E)$ by tuning the strength of a central barrier and the applied magnetic field, below we show the conductance as a function of

$$X = \frac{E}{\hbar\Omega_w} + \frac{1}{2}. \quad (6)$$

The integer part of the parameter X counts how many propagating channels in the wire are open for an incoming electron with energy E .

A. Tuning the central barrier

In Fig. 2, we investigate the tuning effects of the central barrier V_2 in a magnetic field $B = 0.5$ T. Correspondingly, the effective magnetic length $a_w = 29.34$ nm and the effective subband separation $\hbar\Omega_w = 1.32$ meV, and hence $a_w = a_{2D} \sqrt{\omega_c/\Omega_w} \simeq 0.8a_{2D}$ with a_{2D} being the magnetic length in a flat two-dimensional system. The center of the side dots are located at $(x_c, y_c) =$

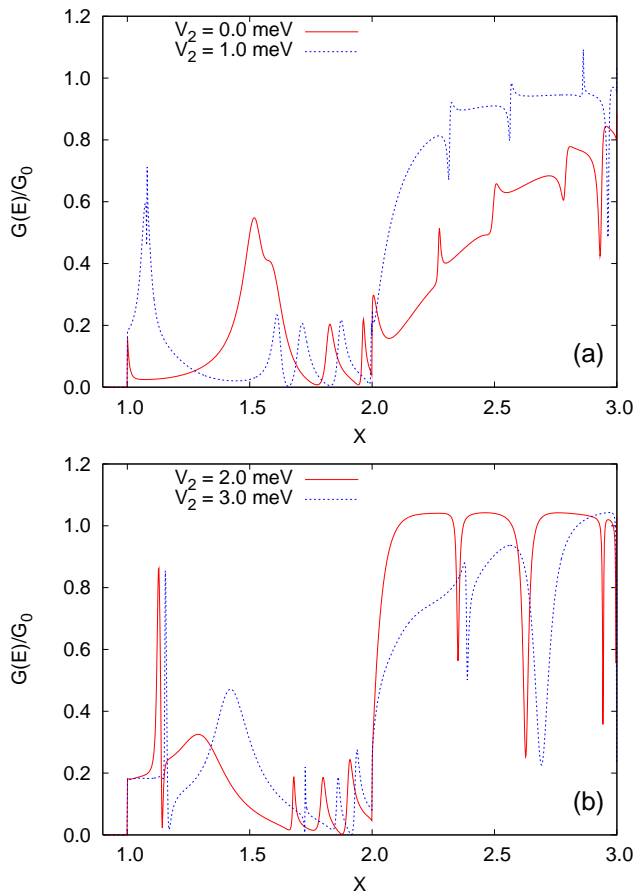


FIG. 2: The conductance in units of $G_0 = 2e^2/h$ as a function of X in a magnetic field $B = 0.5$ T with different height of the central barrier $V_2 =$ (a) 0.0 (solid), and 1.0 (dashed) meV; (b) 2.0 (solid), and 3.0 (dashed) meV. Other parameters are $V_1 = V_3 = -6.0$ meV and $L = 4.82a_w$.

($0, \pm 3.4a_w$). Since the magnetic field at 0.5 Tesla provides an optimal condition to facilitate the UD-LD coupling and enhance a cyclotron backscattering, the general features in G are strongly suppressed due to a *magnetic blocking* effect. In the single-mode regime ($1 < X < 2$), this magnetic blocking effect becomes significant in the high kinetic energy (KE) regime. In the double-mode regime ($2 < X < 3$), if the height of the central barrier is close to $\hbar\Omega_w$ (such as $V_2 = 1.0$ and 2.0 meV) [see Fig. 2], the magnetic blocking effect would be suppressed and the conductance envelop manifests a plateau-like structure at $G/G_0 \approx 1.0$.

In the low-KE single-mode regime, we find sharp Fano-type peaks³⁷ in G : They are at $X = 1.081$ for $V_2 = 1.0$ meV, $X = 1.129$ for $V_2 = 2.0$ meV, and $X = 1.155$ for $V_2 = 3.0$ meV. These structures represent resonant transmission of electrons with continuous subband energy in the leads that strongly couple to the discrete level in the UD forming a long-lived quasibound state with quantum number $(n_x, n_y) = (1, 2)$ in the UD.⁸ It is important to point out that the clockwise cyclotron motion in the

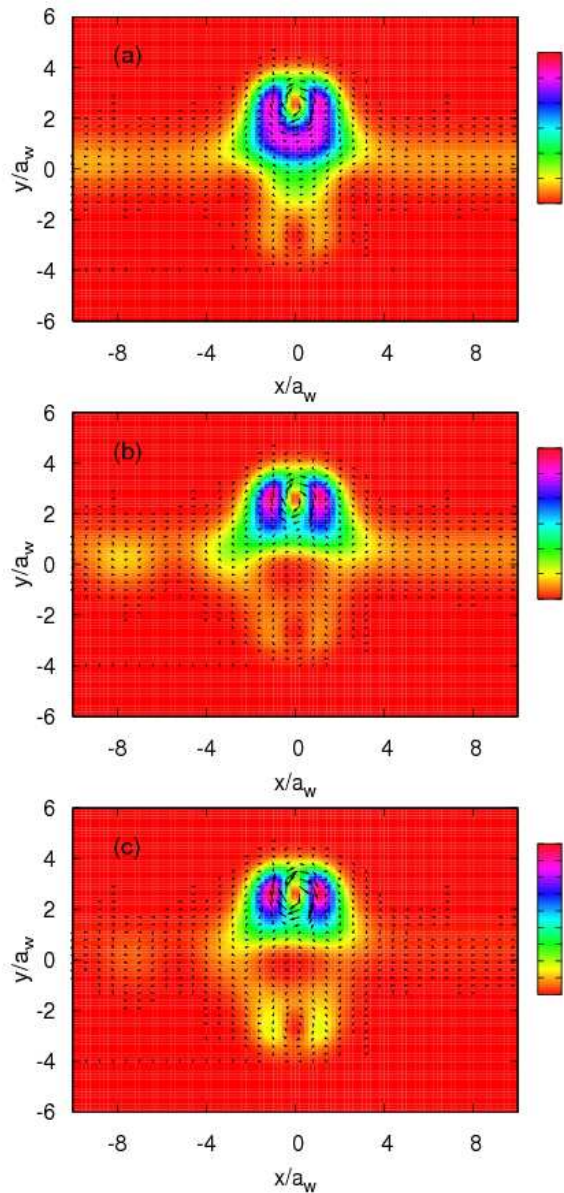


FIG. 3: Probability density and electron current density (black arrows) are plotted as functions of x and y in a magnetic field $B = 0.5$ T with different strength of the central barrier in the low-KE single-mode regime: (a) $V_2 = 1.0$ meV at $X = 1.081$; (b) $V_2 = 2.0$ meV at $X = 1.143$; and (c) $V_2 = 3.0$ meV at $X = 1.171$. Other parameters are $V_1 = V_3 = -6.0$ meV and $L = 4.82a_w$.

UD indicates a *magnetic hole-like state*. These states are shifted by changing V_2 because of the tilting effect to the dot potential by the central barrier. Moreover, the Fano peak with $G/G_0 = 0.71$ at $X = 1.081$ for the case of $V_2 = 1.0$ meV is actually a weak dip-and-peak structure. This weaker structure imposed on the peak is due to the lower central barrier such that the electrons may have stronger coupling to the LD. When the central barrier is tuned to be higher, e.g. 2.0 or 3.0 meV,

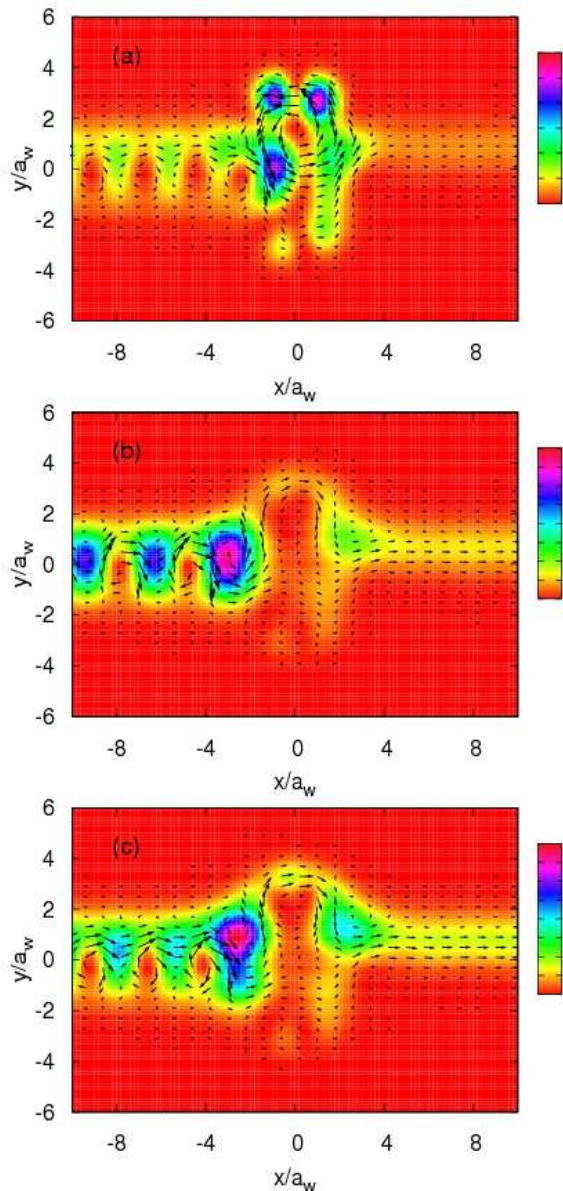


FIG. 4: Probability density and electron current density (black arrows) are plotted as functions of x and y in a magnetic field $B = 0.5$ T with different strength of the central barrier in the mediate-KE single-mode regime: (a) $V_2 = 0.0$ meV at $X = 1.52$; (b) $V_2 = 2.0$ meV at $X = 1.29$; and (c) $V_2 = 3.0$ meV at $X = 1.42$. Other parameters are $V_1 = V_3 = -6.0$ meV and $L = 4.82a_w$.

a perfect (2,1)-like quasibound state can be constructed in the UD, and the conductance manifests strong peak-and-dip structures. On the other hand, there are Fano dips at $X = 1.079$ for $V_2 = 1.0$ meV, $X = 1.143$ for $V_2 = 2.0$ meV, and $X = 1.171$ for $V_2 = 3.0$ meV. These structures correspond to electrons coupled with higher probability to the LD forming a hole-like state, and then being backscattered to the left lead resulting in a conductance dip.

In the mediate-KE single-mode regime, there is a hump structure in G except for the case of $V_2 = 1.0$ meV. The broad nature of these structures implies the short electron dwell time of the quasibound states in the UD. To probe this transport mechanism, we plot the probability density and electron current density in real space shown in Fig. 4. Without a central barrier, the electrons are easily coupled to the LD and then doing cyclotron motion coupled backward with alignment to the second quasibound state in the UD causing a resonant transmission [see Fig. 4(a)]. For $V_2 = 1.0$ meV such an alignment in energy disappears, as a result no hump structure can be found. When the strength of the central barrier increases [see Fig. 4(b)-(c)], the electron energy is gradually allowed to align the first quasibound state energy in the UD to facilitate a resonant transmission. It is interesting to mention that for the case of $V_2 = 0$ meV the shoulder of the hump structure at $X = 1.58$ corresponds to a resonant transmission with lateral tunneling through the central barrier weakly coupling to the LD as displayed in Fig. 5(a).

Now we turn to discuss the high-KE single-mode regime. The general transport characteristics are small peaks in G with height around $0.2G_0$. In this regime, electrons are allowed to strongly couple to the LD. For the case without a central barrier, the electrons at energy $X = 1.83$ form a (1,2)-like quasibound state in the parallel DOQD system as is shown in Fig. 5(b). The second small peak ($X = 1.97$) in G corresponds to a mixed (2,2)-like quasibound state [see Fig. 5(c)]. This state is constructed by four localized electronic cyclotron orbits—two stronger in front of and behind the central barrier and two weaker around the UD and the LD—to form a *hole-like quasibound state* at the center of the DOQD system.

If we increase the height of the central barrier to $V_2 = 2.0$ meV, we find that there are three small resonant peaks in G at $X = 1.68, 1.80,$ and 1.91 . Their corresponding transport patterns in real space are shown in Fig. 6. The first small peak at $X = 1.68$ is a perfect (2,2)-like quasibound state⁸ as demonstrated in Fig. 6(a). We note that there are two valley structures, on the sides of this resonant peak, with conductance minima at $X = 1.66$ and 1.76 . At these incident energies, the electrons only have good coupling to the UD due to the Lorentz force induced shifting effect. When the electrons are well-coupled to the whole DOQD system, such shifting effect becomes unimportant and the transport feature exhibits a clear resonant peak in G .

In Fig. 6(b), we show the electronic transport behavior at the second small peak ($X = 1.80$). It is clearly seen that the counterclockwise cyclotron orbits are separated symmetrically by the central barrier. Due to the Lorentz force, the electrons are able to laterally tunnel through the central barrier spending more time on each side of the barrier thus forming a (1,2)-like quasibound state. With higher incident energy $X = 1.91$, not only the tunneling feature of the UD-LD coupling is present, the electrons

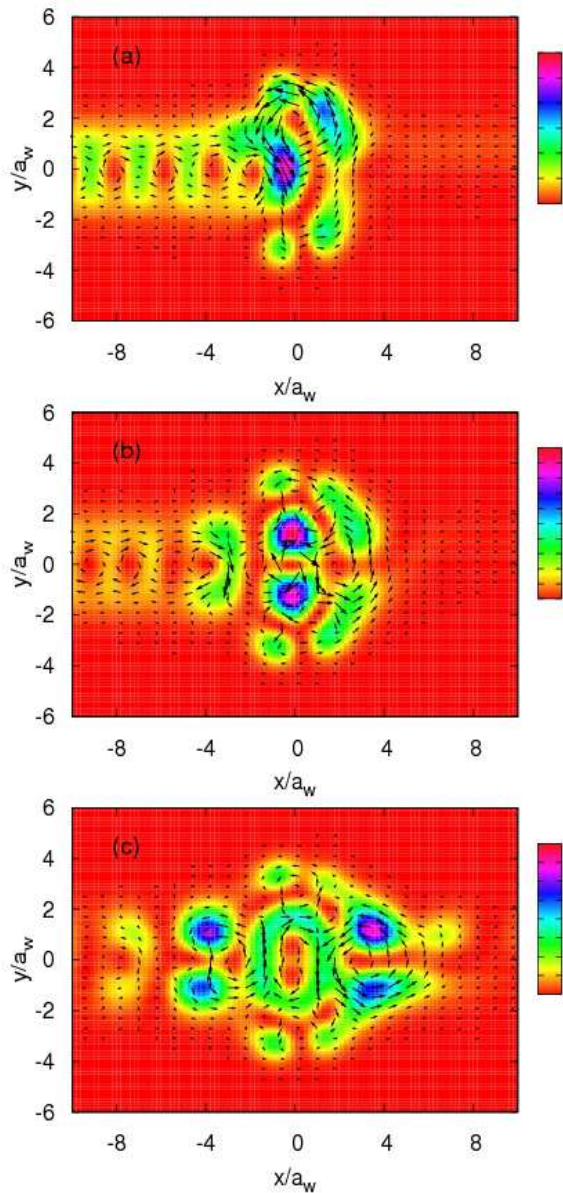


FIG. 5: Probability density and electron current density (black arrows) for the case of $V_2 = 0$ meV and $B = 0.5$ T at $X =$ (a) 1.58; (b) 1.83; and (c) 1.97. Other parameters are $V_1 = V_3 = -6.0$ meV and $L = 4.82a_w$.

are also able to do cyclotron motion bypassing the central barrier [see Fig. 6(c)]. It is interesting to mention in passing that the small peaks at $X = 1.61, 1.71,$ and 1.87 for the case of $V_2 = 1.0$ meV as well as the small peaks at $X = 1.73, 1.86,$ and 1.94 for the case of $V_2 = 3.0$ meV have transport features similar to those of $V_2 = 2.0$ meV.

In contrast to the single-mode regime, one can find a conductance peak in the low-KE double-mode regime only for the case of $V_2 = 0$ meV at $X = 2.01$ [see the solid curve in Fig. 2(a)]. This peak structure indicates a resonant transmission with coupling to the lowest quasi-bound state in the UD. For this case without a cen-

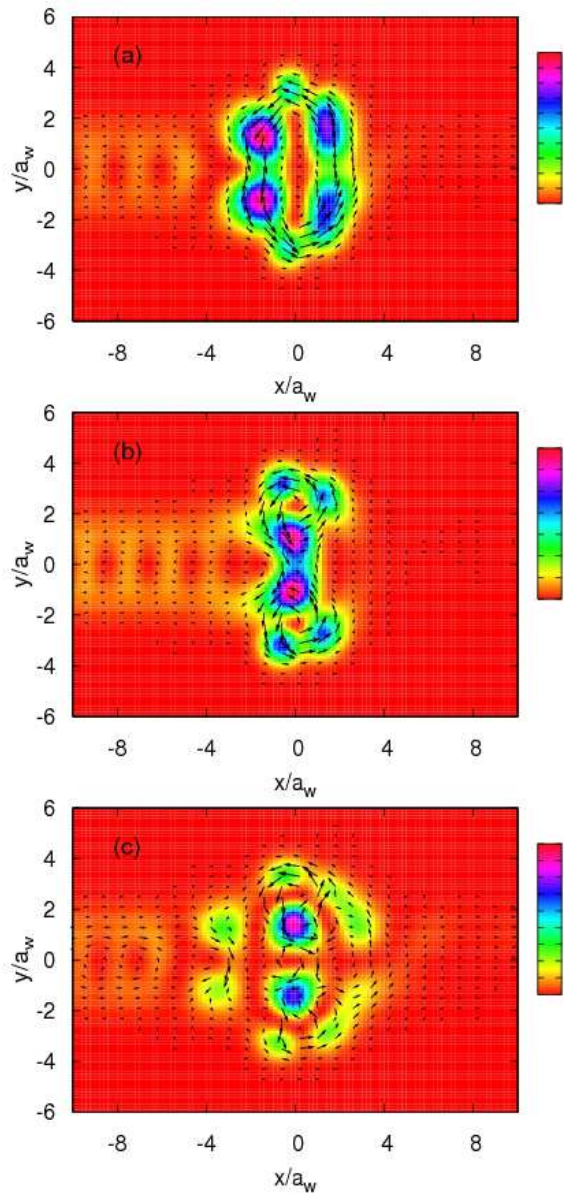


FIG. 6: Probability density and electron current density (black arrows) for the case of $V_2 = 2.0$ meV and $B = 0.5$ T at $X =$ (a) 1.68; (b) 1.80; and (c) 1.91. Other parameters are the same as Fig. 5.

tral barrier and in the mediate-KE double-mode regime, there are two small peak structures in G . First, a resonant transmission due to a magnetic Fabry-Pérot-type resonance in the upper open quantum dot in the upper incident channel is found at $X = 2.28$ forming a resonant peak structure in G as is clearly demonstrated in Fig. 7(a). The electrons in the lower channel transport directly through the DOQD system with coupling to the upper channel. On the other hand, electrons with incident energy $X = 2.51$ manifests a smaller peak structure in G that implies a short-lived resonant state. Figure 7(b) shows that the transport mechanism of this small peak

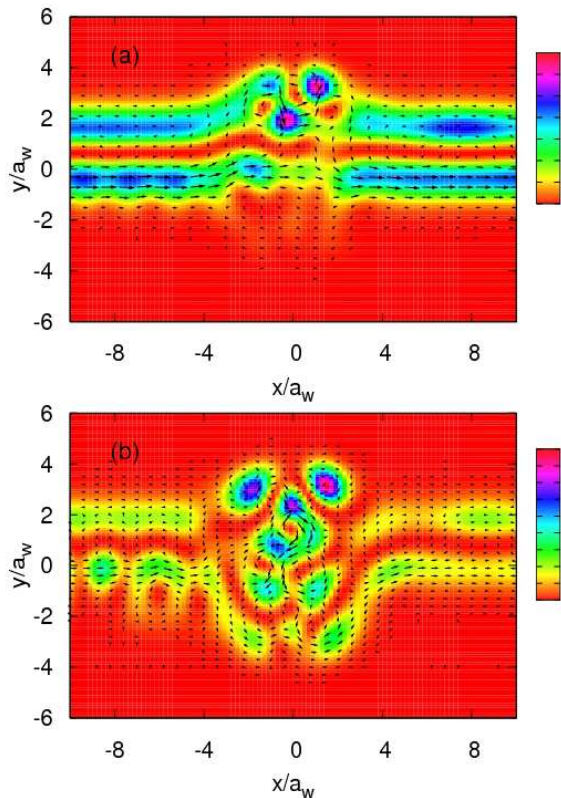


FIG. 7: Probability density and electron current density (black arrows) for the case of $V_2 = 0$ meV and $B = 0.5$ T at $X =$ (a) 2.28 and (b) 2.51. Other parameters are $V_1 = V_3 = -6.0$ meV, $L = 4.82a_w$, and incident mode $n = 1$.

structure is nontrivial: The electrons can form a (2,1)-like quasibound state in the UD with *magnetic turbulence* in the central part of the wire and weakly coupling to the LD. A more complicated magnetic turbulence feature can be found if electrons are incident from the first mode ($n = 0$), due to their higher electron kinetic energy.

Contrarily, for $V_2 = 1.0$ meV in the mediate-KE double-mode regime, there are two small dip structures in G at $X = 2.31$ and 2.56. First, the electrons with incident energy $X = 2.31$ prefer to do a round trip motion around the central barrier forming a strong UD-LD coupling to construct a perfect quasibound state in the parallel DOQD system as depicted in Fig. 8(a). In addition, a weaker peak is found at $X = 2.56$ indicating a shorter living quasibound state. Indeed, as shown in Fig. 8(b), both the probability density and the electron current density are complicated indicating a mixed resonant feature in transport. A resonant state is formed at the central part of the DOQD system with stronger coupling to the UD and weaker coupling to the LD due to the applied magnetic field in \hat{z} direction.

Now we turn to discuss the case of $V_2 = 1.0$ meV in the high-KE double-mode regime. There are two resonant features in G : A small sharp peak at $X = 2.86$ and a deep sharp dip at $X = 2.96$ [see the dashed curve in

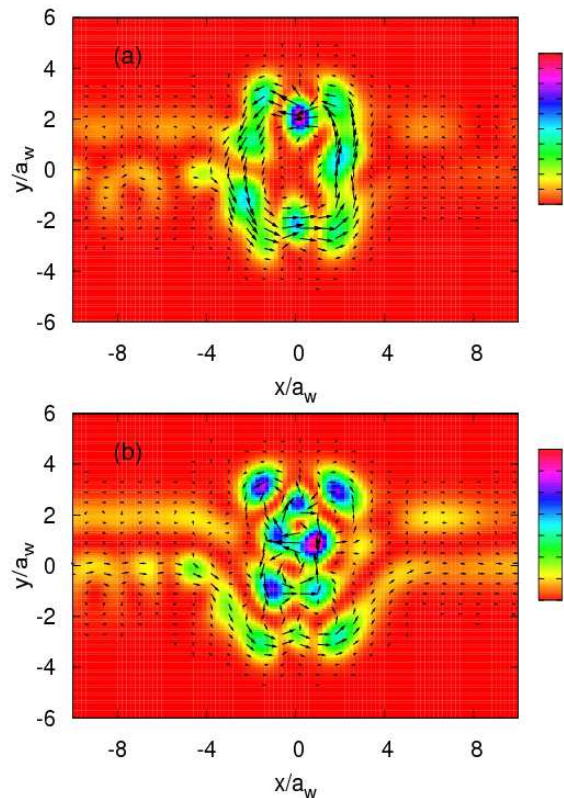


FIG. 8: Probability density and electron current density (black arrows) for the case of $V_2 = 1.0$ meV and $B = 0.5$ T at $X =$ (a) 2.31 and (b) 2.56. Other parameters are the same as Fig. 7.

Fig. 2(a)]. The sharpness of the two structures implies a pure and long-lived resonant state. First, electrons with incident energy $X = 2.86$ are able to construct a hole-like resonant state at the upper central part of the parallel DOQD system as illustrated in Fig. 9(a). Specifically, the electrons have two channels incident from the left lead, that can either couple to the LD or being backscattered to the UD. Those electrons transported through the LD can turn back due to the cyclotron motion and then couple to the UD. Again, electrons may be backscattered by the UD and then coupled to the central barrier. As such, the electrons construct a *magnetic hole-like state* in the DOQD system. Second, the sharp dip in G at $X = 2.96$ implies that a long-lived pure quasibound state is formed in the DOQD system. Indeed, as shown in Fig. 9(b), the probability density shows a (2,3)-like quasibound state constructed in the system, and the weak link to the left and the right lead indicates the long dwell time of this resonant state. Moreover, the electron current density forms a perfect circular motion around the parallel DOQD indicating a pure quasibound state.

Correspondingly, for the case of $V_2 = 0$ meV in the high-KE double-mode regime, there are two structures in G : a shallow dip at $X = 2.78$ and a deep sharp dip at $X = 2.93$ [see the solid curve in Fig. 2]. The correspond-

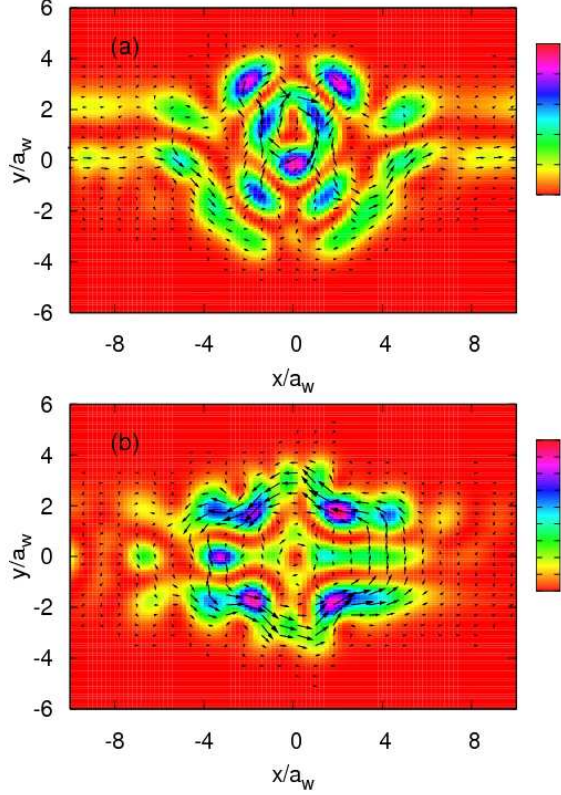


FIG. 9: Probability density and electron current density (black arrows) for the case of $V_2 = 1.0$ meV in the high-KE double-mode regime in a magnetic field $B = 0.5$ T at $X =$ (a) 2.86 and (b) 2.96. Other parameters are $V_1 = V_3 = -6.0$ meV, $L = 4.82a_w$, and incident mode $n = 1$.

ing probability density and the electron current density distribution of these two resonance states are similar to the case of $V_2 = 1.0$ meV in the high-KE double-mode regime. However, unlike the small sharp peak in G at $X = 2.86$ for the case of $V_2 = 1.0$ meV, electron transport with shallow dip in G at $X = 2.78$ for the case of $V_2 = 0$ meV is not able to form a hole-like bound state due to the absence of backscattering from the central barrier. Instead, electron can form a quasibound state at the center of the parallel DOQD system. The sharp dip in G at $X = 2.93$ corresponds to a pure (2,3)-like quasibound state, which is similar to the dip structure at $X = 2.96$ for the case of $V_2 = 1.0$ meV. The similarity of the transport features is due to the large loop of the symmetric cyclotron motion. Therefore, the central barrier plays an insignificant role for such a transport feature. Furthermore, the three probability density peaks in the transverse direction imply that this (2,3)-like quasibound state is caused by the vicinity of the third subband threshold in the leads.

We now discuss the case of $V_2 = 2.0$ meV in the double-mode regime, there are three significant deep and sharp dips in G as displayed by the solid curve in Fig. 2(b). The first two sharp dips are at $X = 2.35$ and 2.63 in

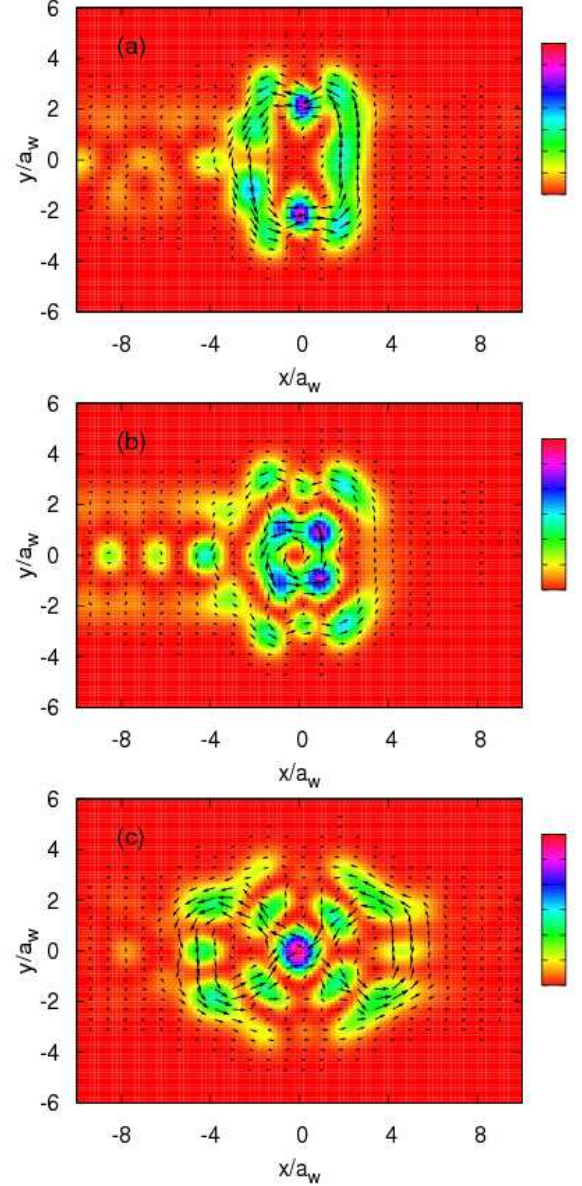


FIG. 10: Probability density and electron current density (black arrows) for the case of $V_2 = 2.0$ meV in the double-mode regime at $X =$ (a) 2.35; (b) 2.63; and (c) 2.94. Other parameters are $B = 0.5$ T, $V_1 = V_3 = -6.0$ meV, $L = 4.82a_w$, and incident mode $n = 1$.

the mediate-KE regime. First, for the case of the dip at $X = 2.35$, the electrons make a perfect (2,1)-like quasibound state with clear cyclotron motion as demonstrated in Fig. 10(a). By tuning the central barrier and the energy of the incident electron to this condition, the UD and the LD can be strongly coupled with a long life time. Second, for the case of dip at $X = 2.63$, the electron probability density forms a double ring structure in real space, and the electron current flows counterclockwise following this double ring loop with interference at the UD and the LD regions as is shown in Fig. 10(b). Such a resonant

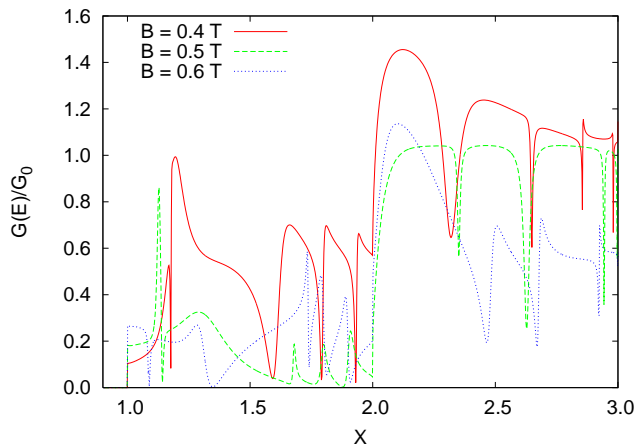


FIG. 11: The conductance in units of $G_0 = 2e^2/h$ as a function of X for a DOQD system with central barrier $V_2 = 2.0$ meV in a magnetic field $B =$ (a) 0.4 T (solid); (b) 0.5 T (dashed); and (c) 0.6 T (dotted). Other parameters are $V_1 = V_3 = -6.0$ meV and $L \simeq 141$ nm.

state formed around the central barrier is a quasibound state with negative binding energy -0.91 meV.³⁴ Turning to the very narrow and deep dip at $X = 2.94$ in the high-KE double-mode regime, the electrons construct a very clear long-living state at the origin in real space as depicted in Fig. 10(c). The transport mechanism is that the electrons make intersubband transitions to the subband top at the origin of the central barrier forming a quasibound state. Two clear cyclotron orbits are seen in front of and behind the central barrier [see Fig. 10(c)].

B. Tuning the magnetic field

Before we discuss the tuning effects on the coherent quantum transport by adjusting the strength of the external perpendicular magnetic field, we would like to mention that due to the complex potential-envelop nature of the laterally parallel DOQD system, there are several relatively short length scales of the system leading to the enhanced sensitivity to magnetic field in the range 0 – 1 Tesla.

Figure 11 shows the magnetic field effects on the conductance to the DOQD system for an appropriate central barrier $V_2 = 2.0$ meV. The strength of the magnetic field is chosen to be $B = 0.4, 0.5,$ and 0.6 T, which correspond, respectively, to the effective magnetic length $a_w = 30.59, 29.34,$ and 29.10 nm; the effective subband separation $\hbar\Omega_w = 1.22, 1.32,$ and 1.44 meV; and the effective length of the DOQD system is $L/a_w = 4.62, 4.82,$ and 4.86 . It is clearly shown in Fig. 11 that, in the single-mode regime, the magnetic blocking effect is most significant for the case of $B = 0.5$ T. On the other hand, in the double-mode regime, the general suppressed plateau feature in the conductance is changed for the case of $B = 0.4$ and 0.6 T: enhanced in the low-KE regime and suppressed in

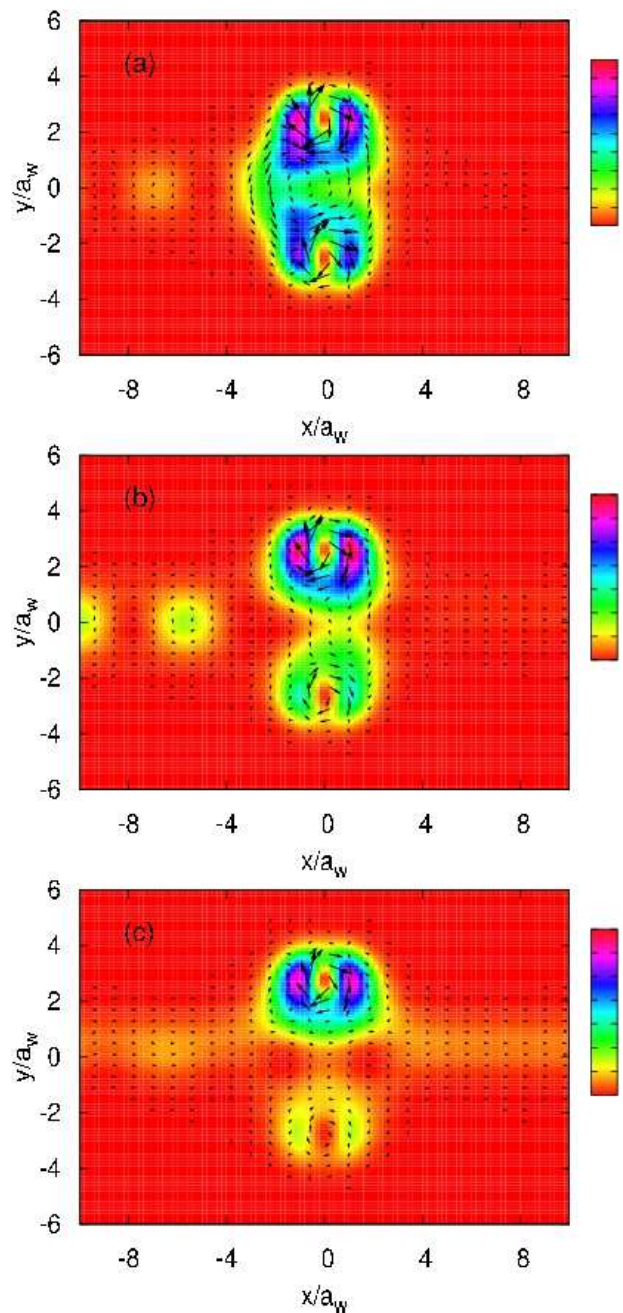


FIG. 12: Probability density and electron current density (black arrows): (a) at $X = 1.18$ for $B = 0.4$ T; (b) at $X = 1.14$ for $B = 0.5$ T; and (c) at $X = 1.09$ for $B = 0.6$ T. Other parameters are $V_2 = 2.0$ meV, $V_1 = V_3 = -6.0$ meV, and $L \simeq 141$ nm.

the high-KE regime.

In the low-KE single-mode regime, there are three sharp downward dips in G at $X = 1.18$ for $B = 0.4$ T (solid), $X = 1.14$ for $B = 0.5$ T (dashed), and $X = 1.09$ for $B = 0.6$ T (dotted). The transport mechanism of these three dips is similar: The incident electron energy has good alignment to the discrete levels in the upper open dot forming a magnetic hole-like (2,1) quasibound

state. For a weaker magnetic field $B = 0.4$ T, the electrons with larger cyclotron orbit can bypass the central barrier, and hence the UD-LD coupling is strong enough to form a symmetric probability density pattern as is shown in Fig. 12(a). Therefore, the conductance manifests a very sharp downward dip in response to this robust effect. When the magnetic field is further increased, the hole-like quasibound state formed in the lower open dot is getting still weaker. This trend is clearly demonstrated in Fig. 12(b)-(c). For the case of $B = 0.5$ T, the mediate UD-LD coupling leads to a clear Fano structure in the conductance [see the dashed curve in Fig. 11]. However, when the magnetic field is increased to $B = 0.6$ T, the UD-LD coupling is further weaker leading to vanishing Fano structure and, instead, the electron conduction manifests a simple dip structure with zero conductance as depicted by the dotted curve in Fig. 11.

Turning to the mediate-KE single-mode regime, there are three significant resonant structures in G [see Fig. 11]: The peak structure at $X = 1.20$ for $B = 0.4$ T, the hump structure at $X = 1.29$ for $B = 0.5$ T, and the valley structure at $X = 1.35$ for $B = 0.6$ T. First, the transport mechanism of the peak structure (for $B = 0.4$ T) is related to the dip structure shown in Fig. 13(a) forming a Fano-like line shape. This peak structure is due to electrons with strong coupling to the upper open dot forming a hole-like (2,1) quasibound state and making resonant transmission [see Fig. 13(a)]. Unlike the dip structure at $X = 1.18$, there is almost no coupling to the lower open dot thus facilitating electron conduction, as coupling to the LD usually enhances backscattering to the left lead. Second, concerning the hump structure for the case of $B = 0.5$ T, the energy alignment to the upper open dot is not present. Hence, the electrons are not easily coupled to the parallel DOQD system. Instead, the electrons form a short-lived quasibound state in front of the central barrier as illustrated with Fig. 13(b). Third, for the case of valley structure at $X = 1.35$ for $B = 0.6$ T, an electron incident from the left reservoir impinges on the central barrier and could either couple to the UD or being transported through the lower part bypassing the central barrier forming a resonance state on the left edge of the system, as is shown in Fig. 13(c). The multiple cyclotron scattering between the two quasibound states, formed on the two edges of the central barrier, may backward tunnel through the central barrier exhibiting a zero conductance at $X = 1.35$ [see the dotted curve in Fig. 11].

It is interesting to mention in passing that, in the mediate-KE single mode-regime, a hole-like quasibound state is constructed in the upper open quantum dot for the case of $B = 0.4$ T. When the magnetic field is increased to 0.5 Tesla, such a hole-like state has vanished. However, for a stronger magnetic field $B = 0.6$ T, the hole-like quasibound state appears again with significant magnetic multiple scattering on the two edges of the parallel DOQD system as is clearly demonstrated in Fig. 13.

For the case of $B = 0.4$ T in the higher kinetic energy single-mode regime, the conductance manifests strong os-

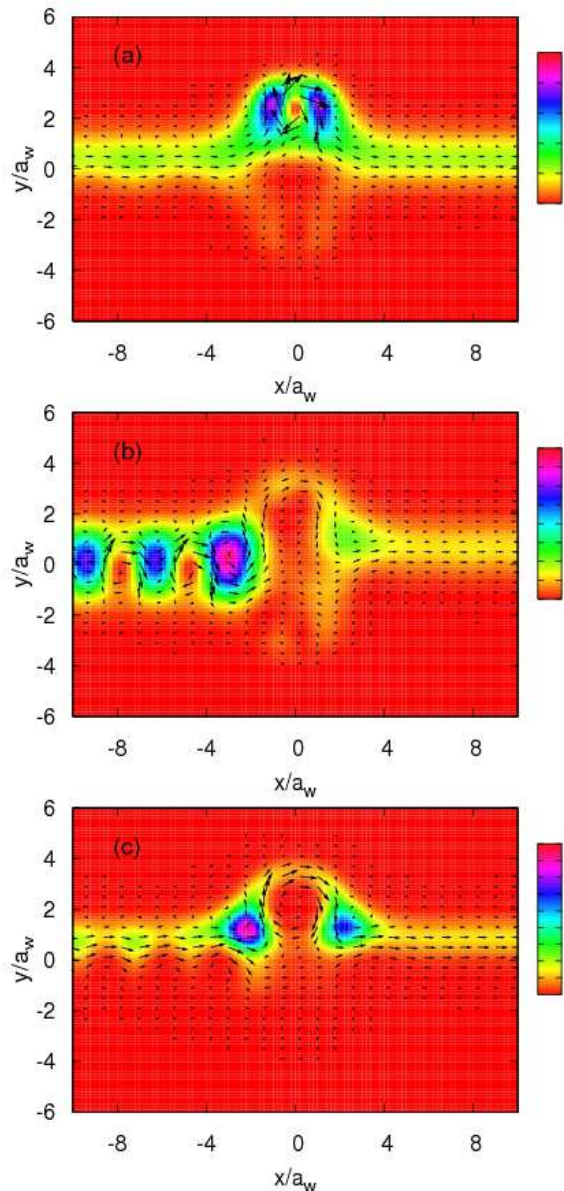


FIG. 13: Probability density and electron current density (black arrows): (a) at $X = 1.20$ for $B = 0.4$ T; (b) at $X = 1.29$ for $B = 0.5$ T; and (c) at $X = 1.35$ for $B = 0.6$ T. Other parameters are $V_2 = 2.0$ meV, $V_1 = V_3 = -6.0$ meV.

cillation effects as shown by the solid curve of Fig. 11. A broad and deep dip structure is found at $X = 1.59$, the electrons incident at this energy are scattered by the central barrier but can perform a big cyclotron orbit through the system with UD-LD coupling and construct a (2,1)-like quasibound state on the right edge of the DOQD system, as demonstrated in Fig. 14. On the other hand, those electrons that are backscattered by the central barrier may interplay with the incident electrons constructing a hole-like quasibound state in front of the central barrier. In Fig. 11, the sharp downward dips at $X = 1.79$ and 1.93 for the case of $B = 0.4$ T have similar probabil-

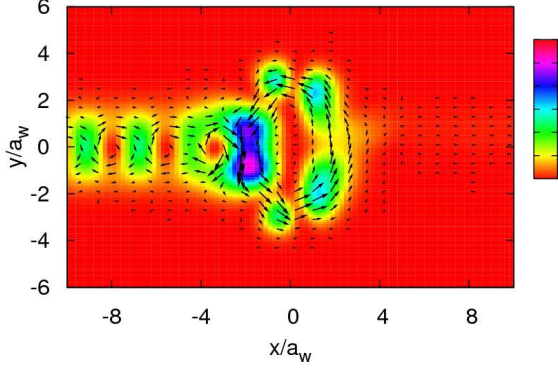


FIG. 14: Probability density and electron current density (black arrows) for the case of $B = 0.4$ T at $X = 1.59$. Other parameters are $V_2 = 2.0$ meV and $V_1 = V_3 = -6.0$ meV.

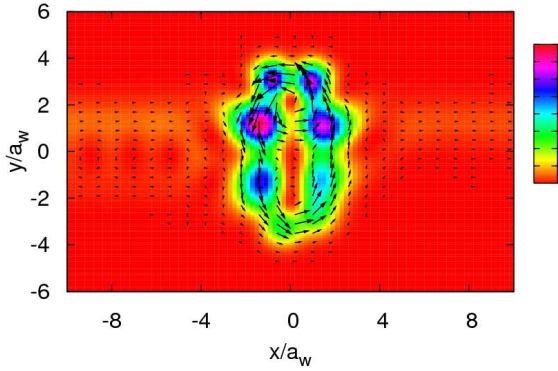


FIG. 15: Probability density and electron current density (black arrows) for the case of $B = 0.6$ T at $X = 1.73$. Other parameters are $V_2 = 2.0$ meV and $V_1 = V_3 = -6.0$ meV.

ity and electron current density patterns to, respectively, the small peaks at $X = 1.80$ and 1.91 for the case of $B = 0.5$ T [see Fig. 6(b)-(c)]. When the magnetic blocking effect is significant, the electronic transport manifests resonant transmission. However, if the magnetic blocking effect is insignificant, the transport feature tends to be resonant reflection.

For a stronger magnetic field, $B = 0.6$ T, the conductance manifests three Fano line-shapes in the high-KE single-mode regime. The transport features for the Fano dips at $X = 1.74$, 1.81 , and 1.91 are very similar to, respectively, the three small dips at $X = 1.68$, 1.80 , and 1.91 for the case of $B = 0.5$ T as is shown in Fig. 6. For the case of $B = 0.6$ T, the transport features of the Fano peaks at $X = 1.79$ and 1.89 are similar to their Fano dips but with stronger coupling to the right lead. However, the transport feature of the first Fano peak at $X = 1.73$ has significant difference with its corresponding Fano dip at $X = 1.74$. The probability density and the electron current density pattern of the Fano peak is shown in Fig. 15. The electrons construct a (2,2)-like quasibound state between the UD and the central bar-

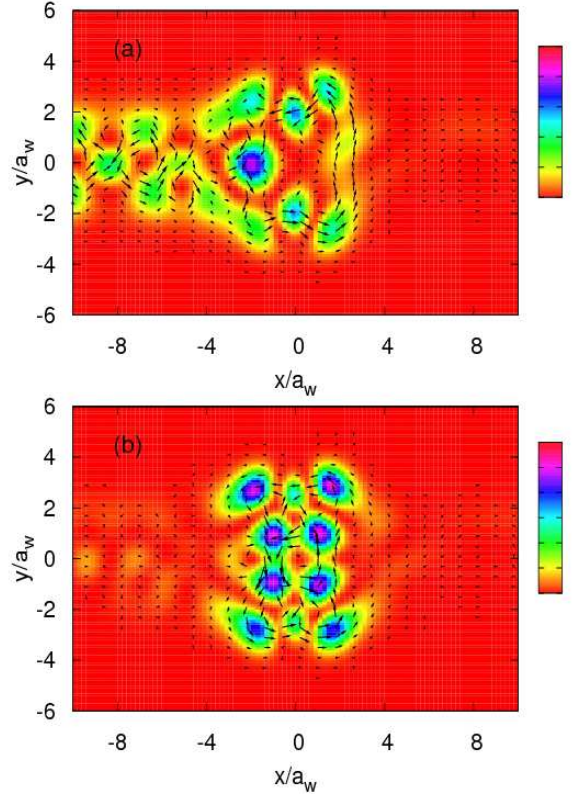


FIG. 16: Probability density and electron current density (black arrows) for the case of $B = 0.4$ T in the mediate-KE double-mode regime at $X =$ (a) 2.32 and (b) 2.65 . Other parameters are $V_2 = 2.0$ meV, $V_1 = V_3 = -6.0$ meV, and incident mode $n = 1$.

rier. In addition, the electrons can also couple to the LD forming a complete cyclotron motion in the whole DOQD system. The weak coupling to the two leads shown in Fig. 15 implies the long dwell time of this quasibound state.

Now we turn to study the transport features in the double-mode regime. In this regime, the conductance manifests significant downward-dip structures implying resonant reflection. For the case of $B = 0.4$ T in the mediate-KE regime, there are two significant dip structures in G at $X = 2.32$ and 2.55 as shown by the solid curve in Fig. 11. When the electrons are incident with energy $X = 2.32$, the wave function scars are found not only in the DOQD but also in the left lead as is shown in Fig. 16(a), this indicates that a strong quantum interference occurs between two propagating channels in the left lead. Moreover, this quantum interference occurring in the lead also implies a metastable quasibound state with a short dwell time, and hence the conductance manifests a broad-dip feature. Furthermore, a strong dot-lead coupling can be found by the high probability density on the left edge of the DOQD system. On the other hand, when the electrons are incident with energy $X = 2.65$, as is clearly demonstrated in Fig. 16(b), they can construct a

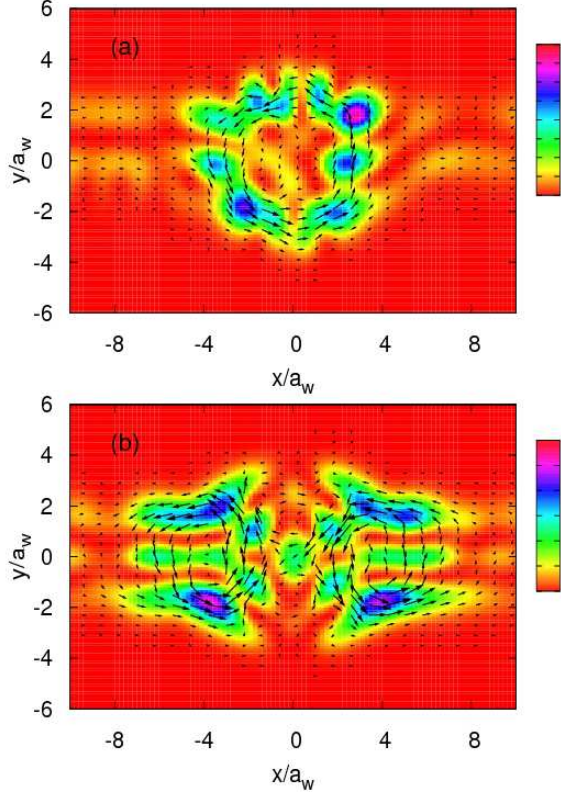


FIG. 17: Probability density and electron current density (black arrows) for the case of $B = 0.4$ T in the high-KE double-mode regime at $X =$ (a) 2.85 and (b) 2.98. Other parameters are $V_2 = 2.0$ meV, $V_1 = V_3 = -6.0$ meV, and incident mode $n = 1$.

perfect (2,4)-like quasibound state in the parallel DOQD system. In addition, this (2,4)-like state can easily couple to the upper and the lower open dot thus accomplishing a highly symmetric probability pattern shown in Fig. 16(b).

For the case of $B = 0.4$ T in the high-KE double-mode regime, there are two narrow sharp dips in G at $X = 2.85$ and 2.98 [see the solid curve in Fig. 11]. When the electrons are incident with energy $X = 2.85$, the electrons have a strong coupling to the parallel DOQD system forming a (2,3)-like quasibound state, and this state has weak coupling to the UD and the LD, as depicted in Fig. 17(a). If the electrons are incident with energy $X = 2.98$, the conductance feature is a very sharp and narrow dip. The electrons can perform intersubband transitions to the threshold of the third subband forming a quasibound state in the left and the right lead as is clearly demonstrated in Fig. 17(b). The two clear cyclotron orbits in front of and behind the DOQD system are found with inversion symmetry implying a long-lived quasibound state. Due to the Lorentz force, such a state formed in the lead may flow back to the system forming (1,2)-like metastable quasibound states either in front of or behind the central barrier, and these two metastable

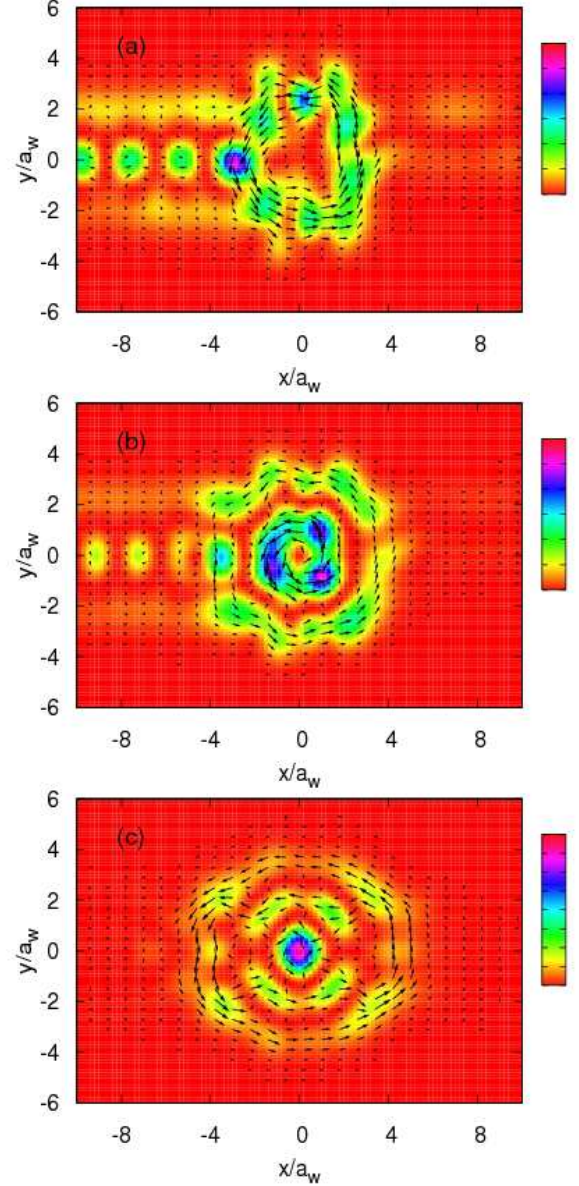


FIG. 18: Probability density and electron current density (black arrows) for the case of $B = 0.6$ T in the double-mode regime at $X =$ (a) 2.47; (b) 2.67; and (c) 2.92. Other parameters are $V_2 = 2.0$ meV, $V_1 = V_3 = -6.0$ meV, and incident mode $n = 1$.

states may have weak coupling through the central barrier.

For a higher magnetic field ($B = 0.6$ T) in the double-mode regime, the transport characteristics exhibit asymmetric dip features in the conductance as is shown by the dotted curve in Fig. 11. These dips are at $X = 2.47, 2.67$, and 2.92 with an opening line-shape in the low-energy part of the dip structure and with an abrupt change in G in the high-energy part of the dip structure. The transport features of the three significant asymmetric dips are displayed in Fig. 18(a)-(c). The general transport fea-

tures of these asymmetric dips are related to the “quantum peg” effect.³⁴

The electrons with incident energy $X = 2.47$, perform a cyclotron-type multiple scattering in the DOQD system with strong constructive quantum interference with incident electron waves on the left edge of the system as is shown in Fig. 18(a). For a higher incident electron energy $X = 2.67$, the cyclotron-type quasibound state has a longer dwell time and the probability pattern displays a double-ring structure. It is clearly demonstrated in Fig. 18(b) that a “quantum peg” structure in real-space probability density is constructed around the central barrier (a quasibound state with negative binding energy). When the incident electron energy is further raised to $X = 2.92$, one can find not only the double-ring structure but also a probability density peak at the origin of the central barrier as is depicted in Fig. 18(c).

The electron current flows dominantly through the outer ring-shaped path indicating a perfect quasibound state constructed around the whole system with long life time. When the electrons flow through the outer ring-shaped path and close to the UD or the LD, they may couple to the dot or turn to couple to the inner ring-shaped state. The low probability density in the UD and the LD implies the electrons traverse directly through the dots. On the other hand, those electrons coupled to the inner path may make intersubband transitions to a localized subband top formed at the origin of the central barrier trapped temporarily forming a quasibound state. This feature is an indirect intersubband transition mechanism similar to the case of $B = 0.5$ T at $X = 2.94$ as is shown in Fig. 10(c).

It is also worth to point out that for the case of $B = 0.6$ T in the double-mode regime, the asymmetric dip structure at $X = 2.92$ is narrower than the other two dips at lower energies, which in reality forms a Fano-type line shape. The Fano-peak at $X = 2.93$ has probability density and electron current density pattern similar to its corresponding Fano-dip at $X = 2.92$, but with stronger coupling to the right lead. The Fano effect is found to be prominent at the same specific magnetic fields such as $B = 0.6$ T, while it is not distinct in the other values. This implies that the coherence nature of the quantum transport through the laterally parallel DOQD system strongly depends on the magnetic field.

IV. CONCLUSIONS

We have demonstrated tunable transport effects of coupling modes in laterally parallel double open quantum dots. In general the applied perpendicular homogeneous magnetic field plays a blocking effect on the quantum transport through the parallel DOQD system. Due to the complex potential-envelop nature of the system, there are several relatively short length scales leading to the sensitivity to magnetic field.

By tuning the central barrier, we have found Fano-type

line-shapes in the conductance in the low-KE single-mode regime. The peaks of these Fano-type line-shapes are magnetic hole-like quasibound-state features in the upper open quantum dot. In the mediate-KE single-mode regime, resonant coupling to the upper open dot is determined by the energy alignment of the incident electron energy with the quasibound levels in the upper quantum dot. In the high-KE single-mode regime, an interesting hole-like quasibound-state feature has been found in the absence of a central barrier by tuning the incident electron energy just below the second subband threshold. Moreover, we have demonstrated the robust features of tunneling through and bypassing the central barrier in the transverse direction to achieve the UD-LD coupling.

In the double-mode regime, we have found a magnetic Fabry-Pérot-type resonant transmission in the upper open dot if the incident kinetic energy is low. In the mediate-KE regime, we have demonstrated the possibility of the magnetic turbulence effect in the central part of the system in the absence of a central barrier. A magnetic hole-like quasibound state feature has been found in the high-KE double-mode regime for a weak central barrier. A clear “quantum peg” structure can be found in the mediate-KE double-mode regime for the case of mediate central barrier. Moreover, in the high-KE double-mode regime, we have found a quasibound state induced by intersubband transitions to the subband top located at the origin of the central barrier.

By tuning the magnetic field, we have found a Fano to downward-dip line-shape crossover on the quantum transport in the low-KE single-mode regime. The magnetic field manipulated energy alignment effect to the upper open dot has also been demonstrated in the mediate-KE single-mode regime. In the high-KE single-mode regime, by increasing the magnetic field from 0.4 Tesla to 0.5 Tesla the conductance features change from downward dips, small peaks, to Fano line-shapes.

In the double-mode regime, the effects of wave function scars and a clear (2,4)-like quasibound state feature have been found for the case of lower magnetic field in the mediate-KE regime. For this lower magnetic field case but with high-KE, the electron transport manifests a (2,3)-like state and a quasibound state trapped at the subband threshold in the leads. When the magnetic field is tuned to be higher, say 0.6 Tesla, the dip structures in the conductance become asymmetric and the transport pattern changes to be “quantum peg” features. When the incident energy is just below the third subband threshold, we can find a robust quasibound state feature formed at the origin of the central barrier.

In summary, we have proposed a laterally parallel DOQD configuration for the investigation of tuning effects upon the coupling modes of lateral parallel quantum dots. Even for such a simple configuration, tuning the coupling modes by the central barrier or by the magnetic field has revealed an essentially complicated nature of coherent quantum transport.

Acknowledgments

The authors acknowledge the financial support by the Research and Instruments Funds of the Icelandic State,

the Research Fund of the University of Iceland, and the Taiwan National Science Council. C.S.T. is grateful to the computational facility supported by the National Center for High-performance Computing in Taiwan.

-
- ¹ A. M. Chang, H. U. Baranger, L. N. Pfeiffer, and K. W. West, *Phys. Rev. Lett.* **73**, 2111 (1994).
- ² H. I. Chan, R. M. Clarke, C. M. Marcus, K. Campman, and A. C. Gossard, *Phys. Rev. Lett.* **74**, 3876 (1995).
- ³ M. Persson, J. Pettersson, B. von Sydow, P. E. Lindelof, A. Kristensen, and K.-F. Berggren, *Phys. Rev. B* **52**, 8921 (1995).
- ⁴ M. W. Keller, A. Mittal, J. W. Sleight, R. G. Wheeler, D. E. Prober, R. N. Sacks, and H. Shrtikmann, *Phys. Rev. B* **53**, R1693 (1996).
- ⁵ Y. Wang, N. Zhu, and J. Wang, *Phys. Rev. B* **53**, 16 408 (1996).
- ⁶ R. Akis, D. K. Ferry, and J. P. Bird, *Phys. Rev. Lett.* **79**, 123 (1997); *ibid.* **81**, 1745 (1998); J. P. Bird, R. Akis, D. K. Ferry, D. Vasileska, J. Cooper, Y. Aoyagi, and T. Sugano, *ibid.* **82**, 4691 (1999); A. P. S. de Moura, Y.-C. Lai, R. Akis, J. P. Bird, and D. K. Ferry, *ibid.* **88**, 6804 (2002).
- ⁷ I. V. Zozoulenko and T. Lundberg, *Phys. Rev. Lett.* **81**, 1744 (1998).
- ⁸ C. S. Tang, Y. H. Tan, and C. S. Chu, *Phys. Rev. B* **67**, 20 5324 (2003).
- ⁹ A. A. Clerk, X. Waintal, and P. W. Brouwer, *Phys. Rev. Lett.* **86**, 4636 (2001).
- ¹⁰ M. G. Vavilov, L. DiCarlo, and C. M. Marcus, *Phys. Rev. B* **71**, 24 1309(R) (2005).
- ¹¹ Y.-H. Kim, M. Barth, U. Kuhl, H.-J. Stöckmann, and J. P. Bird, *Phys. Rev. B* **68**, 04 5315 (2003).
- ¹² M. Mendoza and P. A. Schulz, *Phys. Rev. B* **71**, 24 5303 (2005).
- ¹³ For a general overview see, e.g., W. G. van der Wiel, S. D. Franceschi, J. M. Elzerman, T. Fujisawa, S. Tarucha, L. P. Kouwenhoven, *Rev. Mod. Phys.* **75**, 1 (2003).
- ¹⁴ J. C. Chen, A. M. Chang, and M. R. Melloch, *Phys. Rev. Lett.* **92**, 17 6801 (2004).
- ¹⁵ H. Lu, R. Lü, and B.-F. Zhu, *Phys. Rev. B* **71**, 23 5320 (2005); R. Lü, Z.-R. Liu, and G.-M. Zhang, *cond-mat/0504288*.
- ¹⁶ G. Kießlich, P. Samuelsson, A. Wacker, and E. Schöll, *cond-mat/0507403*.
- ¹⁷ T. H. Oosterkamp, T. Fujisawa, W. G. van der Wiel, K. Ishibashi, R. V. Hijman, S. Tarucha, and L. P. Kouwenhoven, *Nature (London)* **395**, 873 (1998).
- ¹⁸ H. Jeong, A. M. Chang, M. R. Melloch, *Science* **293**, 2221 (2001).
- ¹⁹ T. Kostyrko and B. R. Bulka, *Phys. Rev. B* **71**, 23 5306 (2005).
- ²⁰ I. Žutić, J. Fabian, and S. Das Sarma, *Rev. Mod. Phys.* **76**, 323 (2004).
- ²¹ R. Requist, J. Schliemann, A. G. Abanov, and D. Loss, *Phys. Rev. B* **71**, 11 5315 (2005).
- ²² A. C. Johnson, C. M. Marcus, M. P. Hanson, and A. C. Gossard, *Phys. Rev. B* **71**, 11 5333 (2005).
- ²³ O. N. Jouravlev and Y. V. Nazarov, *cond-mat/0507680*.
- ²⁴ T. Kuzmenko, K. Kikoin, and Y. Avishai, *Phys. Rev. Lett.* **89**, 15 6602 (2002).
- ²⁵ U. Hartmann and F. K. Wilhelm, *Phys. Rev. B* **69**, 16 1309(R) (2004).
- ²⁶ G.-H. Ding, C. K. Kim, and K. Nahm, *Phys. Rev. B* **71**, 20 5313 (2005).
- ²⁷ I.V. Zozoulenko, A.S. Sachrajda, C. Gould, K.-F. Berggren, P. Zawadzki, Y. Feng, and Z. Wasilewski, *Phys. Rev. Lett.* **83**, 1838 (1999).
- ²⁸ V. Gudmundsson, Y. Y. Lin, C. S. Tang, V. Moldoveanu, J. H. Bardarson, and A. Manolescu, *Phys. Rev. B* **71**, 23 5302 (2005).
- ²⁹ V. Gudmundsson, G. Gudmundsdottir, J. H. Bardarson, I. Magnusdottir, C. S. Tang, and A. Manolescu, *Eur. Phys. J. B* **45**, 339 (2005).
- ³⁰ M. C. Rogge, F. Cavaliere, M. Sassetti, R. J. Haug, B. Kramer, *cond-mat/0507036*.
- ³¹ C. S. Chu and R. S. Sorbello, *Phys. Rev. B* **40**, 5941 (1989); P. F. Bagwell, *ibid.* **41**, 10354 (1990); S. A. Gurvitz and Y. B. Levinson, *ibid.* **47**, 10578 (1993).
- ³² J. Faist, P. Guéret, and H. Rothuizen, *Phys. Rev. B* **42**, 3217 (1990).
- ³³ R. B. Laughlin, *Phys. Rev. B* **27**, 3383 (1983).
- ³⁴ V. Gudmundsson, C. S. Tang, and A. Manolescu, *cond-mat/0506009*.
- ³⁵ C. S. Tang and C. S. Chu, *Phys. Rev. B* **53**, 4838 (1996); *ibid. Physica B* **254**, 178 (1998); *ibid. Phys. Rev. B* **60**, 1830 (1999); *ibid. Physica B* **292**, 127 (2000).
- ³⁶ S. A. Gurvitz, *Phys. Rev. B* **51**, 7123 (1995).
- ³⁷ U. Fano, *Phys. Rev.* **124**, 1866 (1961); U. Fano, *Nuovo Cimento* **12**, 156 (1935).